

# The three-dimensional distributions of Type II Cepheids and Anomalous Cepheids in the Magellanic Clouds. Do these stars belong to the old, young or intermediate-age population?

P. Iwanek<sup>1†</sup>, I. Soszyński<sup>1</sup>, A. Udalski<sup>1</sup>, M. K. Szymański<sup>1</sup>, S. Kozłowski<sup>1</sup>, P. Pietrukowicz<sup>1</sup>,  
D. Skowron<sup>1</sup>, J. Skowron<sup>1</sup>, P. Mróz<sup>1</sup>, R. Poleski<sup>2,1</sup> and A. Jacyszyn-Dobrzyniecka<sup>1</sup>

<sup>1</sup> Warsaw University Observatory, Al. Ujazdowskie 4, 00-478 Warsaw, Poland

<sup>2</sup> Department of Astronomy, Ohio State University, 140 W. 18th Ave., Columbus, OH 43210, USA

<sup>†</sup> Corresponding author: piwanek@astrouw.edu.pl

## Abstract

The nature of Type II Cepheids and Anomalous Cepheids is still not well known and their evolutionary channels leave many unanswered questions. One of the characteristic features directly related to the age of stars is their spatial distribution. We use complete collection of classical pulsating stars in the Magellanic Clouds discovered by the OGLE project, to compare their spatial distributions. In this analysis we use 9649 Classical Cepheids (DCEPs), 262 Anomalous Cepheids (ACEPs), 338 Type II Cepheids (T2CEPs) and 46 443 RR Lyrae stars (RR Lyr) from both Magellanic Clouds. We compute three-dimensional Kolmogorov-Smirnov tests for every possible pair of T2CEPs and ACEPs with DCEPs, and RR Lyr stars. We confirm that BL Her stars are as old as RR Lyr variables – their spatial distributions are similar, and they create a vast halo around both galaxies. We discover that spatial distribution of W Vir stars has attributes characteristic for both young and old stellar populations. Hence, it seems that these similarities are related to the concentration of these stars in the center of the Large Magellanic Cloud, and the lack of a vast halo. This leads to the conclusion that W Vir variables could be a mixture of old and intermediate-age stars. Our analysis of the three-dimensional distributions of ACEPs shows that they differ significantly from DCEPs. Statistical tests of ACEPs distributions with RR Lyr distributions give ambiguous results. We consider that these two distributions can be similar through the vast halos they create. This similarity would confirm ACEPs evolution scenario that assumes coalescence of a binary system.

## 1 Introduction

Many years of research of the pulsating stars, including famous discovery of the period-luminosity (P–L) relation (Leavitt & Pickering, 1912), made classical pulsators the primary distance indicators in the nearby Universe. Subsequent discoveries of pulsating stars led to the distance scale revision done by Baade (1952), who noted that there are two different groups of Cepheids which follow different P–L relations. Hence, the Cepheids were divided into Population I (called Classical Cepheids; DCEPs) and Population II (called Type II Cepheids; T2CEPs). Nowadays, T2CEPs are divided into three subgroups depending on their pulsation period  $P$ : BL Herculis (BL Her;  $P < 4$  d), W Virginis (W Vir;  $4 \text{ d} \leq P < 20$  d) and RV Tauri (RV Tau;  $P > 20$  d). The boundaries in the pulsation periods for these stars are not strict, and these groups partly overlap. Additionally, Soszyński et al. (2008) distinguished a fourth subgroup of T2CEPs, named peculiar W Virginis stars (peculiar W Vir).

After over sixty years of study of T2CEPs their origin and evolution channels are still not clear. The first evolution scenarios of these stars were proposed by Gingold (1976, 1985). The most up-to-date review of the T2CEPs properties has been done by Welch (2012). It is believed that these objects are low-mass stars belonging to the halo and old disk stellar populations. BL Her stars evolve from blue horizontal giant branch to asymptotic giant branch. During evolution these stars become brighter and their radii increase, which is associated with helium burning in the cores. BL Her variables pass through the instability strip at luminosities, which correspond to the pulsation periods shorter than 4 days. RV Tau variables are post-asymptotic giant branch stars just before the outer envelope expulsion, which is supposed to form a planetary nebula, and a core that becomes a white dwarf. These stars pass through the high-luminosity extension of the Cepheid instability strip which correspond to pulsation periods longer than 20 days. The origin of W Vir stars is the most incomprehensible. It is believed that these variables are asymptotic giant branch stars that have exhausted helium in their cores, and they start burning helium in the shell. The helium burning in the shell causes a gradual reduction of the energy supply from the hydrogen shell, and it turns off. The hydrogen shell re-switches on occur due to the heating caused by gravitational energy. These behaviors in both shells cause blue loops into the instability strip. The loops are expected only

in stars with small enough external envelop, and they could be recurring (Cassisi & Salaris, 2013). Unfortunately, so far there is no evolutionary model which explains such a behavior (Groenewegen & Jurkovic, 2017a).

Soszyński et al. (2008) found evidence that peculiar W Vir stars have companions. Their pulsations are probably caused by the evolution in the binary system. Up-to-date, 50% of known peculiar W Vir stars from the Magellanic Clouds have clear signs of binarity in the light curves.

In Figure 1, we present distributions of T2CEPs in the sky. Positions of BL Her and W Vir stars show a large scatter in both Magellanic Clouds. RV Tau stars seem to be more concentrated around the centers of the Large Magellanic Cloud (LMC) and Small Magellanic Cloud (SMC). Peculiar W Vir stars have slightly different positions in the sky than other T2CEPs – they are mostly clumped around the bar of the LMC and they are located in the center of the SMC. In addition, T2CEPs are found in globular clusters in the LMC, with exception of peculiar W Vir stars (Matsunaga et al., 2009). All these properties suggest that BL Her, W Vir and RV Tau variables very likely belong to the old population, while peculiar W Vir stars may be younger.

Observations of dwarf galaxies in the 50s and 60s of the 20th century showed the existence of another group of pulsating stars, which brightness variations did not match any of the known groups (Thackeray 1950). For this reason this group has been called Anomalous Cepheids (ACEPs; Zinn & Searle 1976). The existence of this group of pulsating stars can be explained in two ways: by evolution of single intermediate-mass, metal-deficient star, which burns helium in the core, or as the effect of coalescence of two old, low-mass stars which evolved in the binary system. Fiorentino & Monelli (2012) found that ACEPs distribution is different than DCEPs or RR Lyr stars distributions. They also suggested that observations of the LMC outskirts could be helpful to solve the problem of ACEPs origin.

In Figure 2, we present sky distribution of ACEPs in the LMC, and SMC. It is clearly seen that these type of pulsating stars create a vast halo around the Clouds. Moreover, there are a few objects in the area between the Magellanic Clouds (called Magellanic Bridge). Therefore, it suggests that these stars belong to the population as old as RR Lyr variables or even older, or they could reside in the Galactic foreground.

In this paper we use our complete collection of pulsating stars discovered in the OGLE-IV data to compare three-dimensional distributions of pulsators in the Magellanic Clouds. Our knowledge about evolutionary status of DCEPs and RR Lyr stars is more complete compared to what we know about T2CEPs or ACEPs. We believe that the comparison of the distributions of T2CEPs and ACEPs with other classical pulsators distributions could throw light on the history and the future of these stars. The spatial distribution of T2CEPs and ACEPs may be a key to understanding their origin.

The paper is organized as follows. In Section 2, we discuss pulsating stars samples selection, which we use in our analysis. The distance determination method used in this paper is presented in Section 3. Section 4 contains a detailed discussion of the method of performing three-dimensional Kolmogorov-Smirnov statistical test, including coordinates transformation to the Cartesian space and Hammer equal-area projection. In Section 5, we debate results of our analysis with probable evolution scenarios for each group of T2CEPs and ACEPs. We compare the decision-making methods in Section 6. Finally, in Section 7 we summarize our results.

## 2 Sample selection

The photometric data obtained by the *Optical Gravitational Lensing Experiment* (OGLE) over 25 years of its activity has allowed to increase the number of known classical pulsating stars by a large factor. At this moment our collection contains 9649 DCEPs, 262 ACEPs, 338 T2CEPs and 46 443 RR Lyr stars in the Magellanic System (Soszyński et al., 2017), which is the most complete and the largest list of classical pulsators in these galaxies. The entire collection is available on-line via FTP site:

<ftp://ftp.astrouw.edu.pl/ogle/ogle4/OCVS/>

Details about the OGLE instrumentation, data reductions, calibrations, sky coverage, and observing cadence can be found in Udalski et al. (2015).

The OGLE collection of DCEPs in the Magellanic Clouds consist of 9649 stars (Soszyński et al., 2015b, 2017). For our analysis we use DCEPs which pulsate solely in the fundamental mode (F-mode; 5229 objects in total) or solely in the first overtone (1O; 3568 objects in total) as the most numerous samples. 2476 of the F-mode and 1775 of the 1O DCEPs are located in the LMC, whereas 2753 F-mode and 1793 1O DCEPs are located in the SMC.

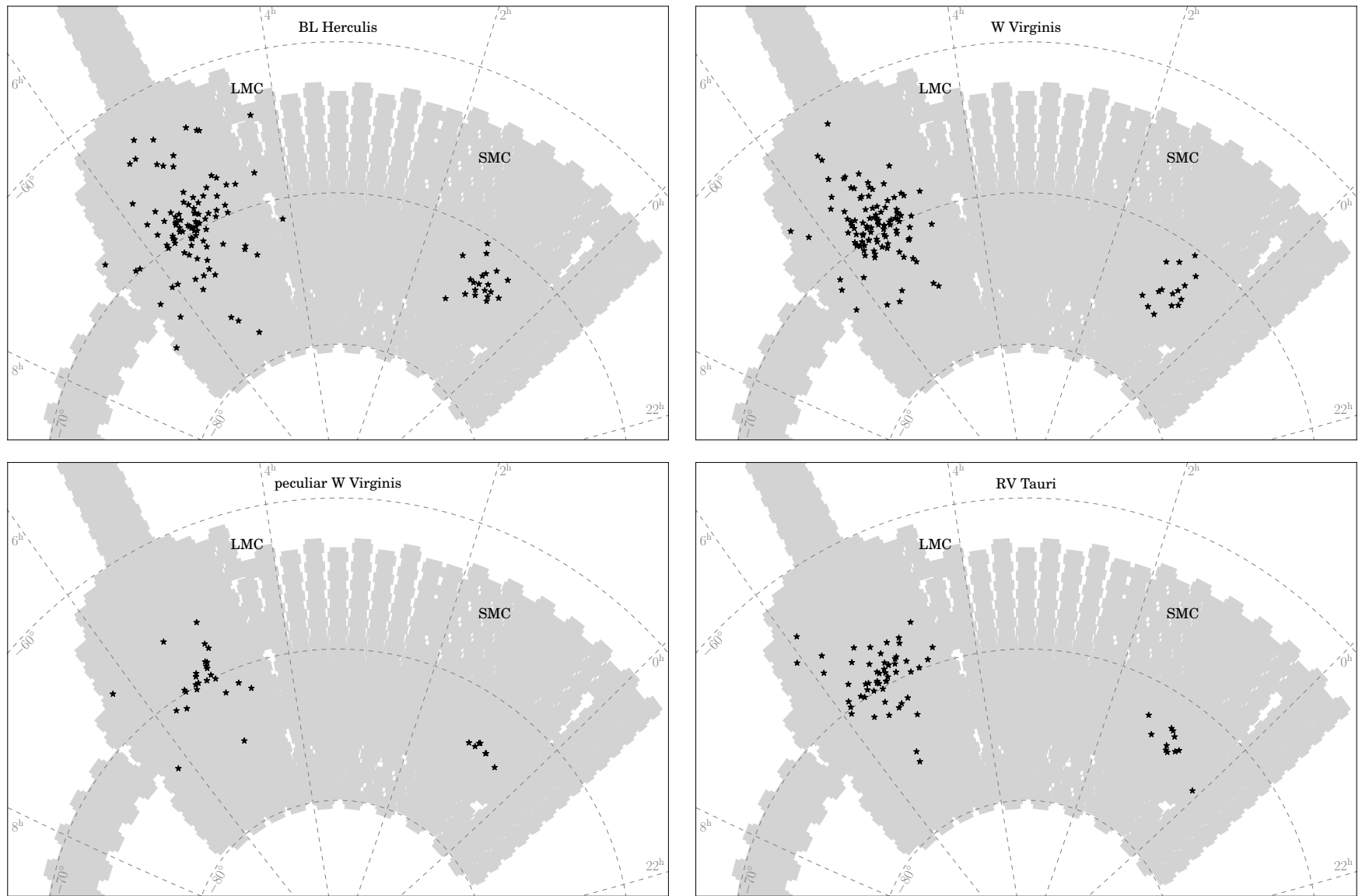


Figure 1: Distributions of Type II Cepheids in the sky. The gray area presents the OGLE-IV footprint.

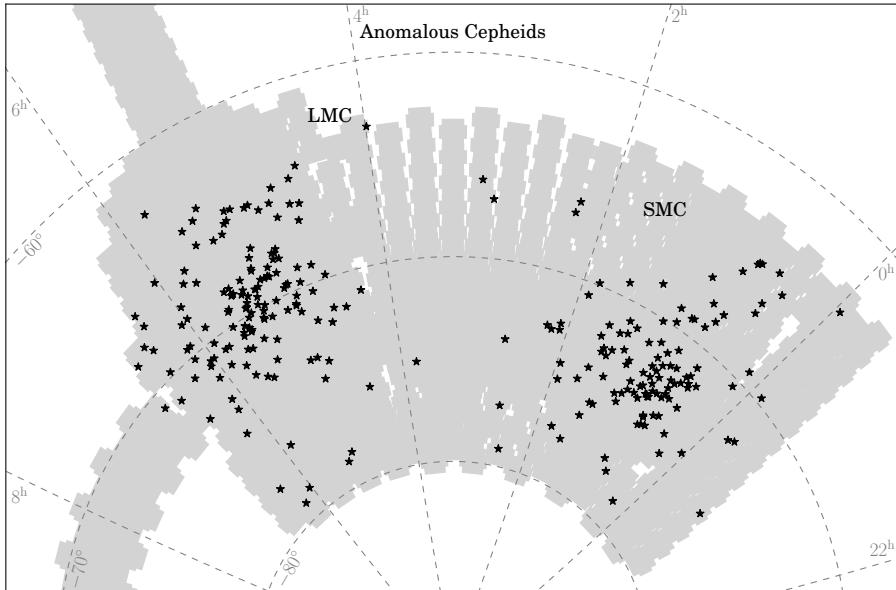


Figure 2: Distributions of Anomalous Cepheids in the sky. The gray area presents the OGLE-IV footprint.

The OGLE sample of pulsating stars consists of 46 443 RR Lyr variables (Soszyński et al., 2016, 2017). We choose RR Lyr stars which pulsate solely in the fundamental mode (RRab; 33 297 objects) or solely in the first overtone (RRc; 10 464 objects). 28 192 RRab stars are located in the LMC and the rest of the sample (5105 objects) are located in the SMC. In the case of the RRc stars we have 9663 objects in the LMC and 801 stars in the SMC. Some of these stars may belong to the Milky Way halo. In the LMC center blending and crowding effects may influence the three-dimensional distribution of RR Lyr stars (Jacyszyn-Dobrzniecka et al., 2017). To partially eliminate blended RRab variables, we reject all objects for which peak-to-peak  $I$ -band amplitudes  $A_I < -5 \cdot \log(P) - 1$ , where  $P$  is the pulsating period in the F-mode (the Bailey diagram, see Fig. 1 in Jacyszyn-Dobrzniecka et al. 2017). After this rejection we are left with 26 681 RRab stars in the LMC and 5018 objects in the SMC.

Our collection of T2CEPs in the Magellanic Clouds contains 338 stars in total (285 stars in the LMC and 53 objects in the SMC; Soszyński et al. 2017, 2018). We subdivide T2CEPs by the pulsation period. In the entire collection, we have 98 BL Her stars in the LMC, and 20 stars in the SMC, 106 W Vir objects in the LMC, and 15 objects in the SMC, and 55 RV Tau stars in the LMC, and 11 such stars in the SMC. The least numerous group is peculiar W Vir stars. Our sample contains 26 these objects in the LMC, and 7 objects in the SMC.

To date, the OGLE project has found 262 ACEPs in the Magellanic System (Soszyński et al., 2015a, 2017). As before, we choose for our analysis stars which pulsate solely in the fundamental mode or solely in the first overtone. 102 F-mode pulsators are located in the LMC, and 78 are located in the SMC. In case of the 10 ACEPs, we have 41 objects in the LMC, and the same number in the SMC.

In Table 1, we present final number of object used in this analysis ( $N_{\text{fin}}$ ) after all selection cuts and after  $\sigma$ -clipping procedure (described in detail in Section 3).

### 3 Determining the distances to the pulsating stars

All of the pulsating stars analyzed in this paper, with the exception of peculiar W Vir stars, follow period–luminosity (P–L) relations, which allow us to calculate their distances. However, P–L relation for RV Tau stars are uncertain due to the large internal scatter along relation, and small number of objects in the Magellanic Clouds. This makes the measured distances to these stars unreliable. For this reason we decide not to carry out the three-dimensional analysis of this T2CEPs subgroup.

We fit P–L relations, separately for every group of pulsating stars listed in Table 1. We use the reddening-independent Wesenheit index (Madore, 1976) defined as follows:

$$W_I = I - 1.55 \cdot (V - I). \quad (1)$$

Table 1: Period–luminosity relations for each type of pulsating stars in the Magellanic Clouds analyzed in this paper.

| Galaxy | Type of stars             | $a$                | $b$                | $N_{\text{fin}}$ |
|--------|---------------------------|--------------------|--------------------|------------------|
| LMC    | F-mode Cepheids           | $-3.319 \pm 0.008$ | $15.892 \pm 0.005$ | 2203             |
|        | 1O Cepheids               | $-3.440 \pm 0.008$ | $15.398 \pm 0.003$ | 1594             |
|        | RRab                      | $-2.975 \pm 0.016$ | $17.167 \pm 0.004$ | 23265            |
|        | RRc                       | $-3.109 \pm 0.026$ | $16.682 \pm 0.013$ | 8376             |
|        | BL Hercules               | $-2.683 \pm 0.091$ | $17.356 \pm 0.024$ | 79               |
|        | W Virginis                | $-2.536 \pm 0.060$ | $17.378 \pm 0.062$ | 94               |
|        | F-mode Anomalous Cepheids | $-2.957 \pm 0.118$ | $16.591 \pm 0.018$ | 94               |
|        | 1O Anomalous Cepheids     | $-3.298 \pm 0.200$ | $16.041 \pm 0.041$ | 39               |
| SMC    | F-mode Cepheids           | $-3.448 \pm 0.011$ | $16.496 \pm 0.005$ | 2565             |
|        | 1O Cepheids               | $-3.570 \pm 0.020$ | $15.969 \pm 0.005$ | 1682             |
|        | RRab                      | $-3.321 \pm 0.063$ | $17.440 \pm 0.014$ | 4378             |
|        | RRc                       | $-3.262 \pm 0.139$ | $16.986 \pm 0.065$ | 639              |
|        | BL Hercules               | $-2.753 \pm 0.403$ | $17.630 \pm 0.104$ | 20               |
|        | W Virginis                | $-2.688 \pm 0.156$ | $17.976 \pm 0.164$ | 15               |
|        | F-mode Anomalous Cepheids | $-2.887 \pm 0.140$ | $16.950 \pm 0.021$ | 72               |
|        | 1O Anomalous Cepheids     | $-3.686 \pm 0.275$ | $16.545 \pm 0.049$ | 39               |

The 1.55 coefficient is calculated from the standard interstellar extinction curve dependence of the  $I$ -band extinction on  $E(V - I)$  reddening (Schlegel et al., 1998). Jacyszyn-Dobrzeniecka et al. (2016) examined Wesenheit index with coefficient 1.44. They found that for these two coefficients there is no significant difference in geometry of the Magellanic System.

Stars that do not have measurements in both  $I$ - and  $V$ -band are rejected from further analysis. Using the Ordinary Least Square method and  $\sigma$ -clipping procedure for each dataset we iteratively fit a linear function in the form:

$$W_I = a \cdot \log(P) + b. \quad (2)$$

In each iteration, we reject points deviating more than  $3\sigma$  from the predicted  $W_I$  until none were rejected. The majority of the rejected outliers are due to blending and crowding effects. The P–L diagrams for all analyzed groups of pulsating stars in the Magellanic Clouds are shown in Figure 3. In Table 1, we present the fitted P–L relations ( $a$  and  $b$  coefficients with appropriate uncertainty) for each dataset with the remaining number of objects ( $N_{\text{fin}}$ ) after all iterations.

We are aware that  $\sigma$ -clipping method is not the most appropriate for studies of three-dimensional distributions as it was shown by Deb et al. (2018) and Nikolaev et al. (2004), that the error distribution is not normal for estimating distances. The application of this method would cause some objects that are genuinely located closer or farther than the entire LMC/SMC sample to be rejected as outliers. However, other studies (i.e. Jacyszyn-Dobrzeniecka et al. 2016, 2017; Inno et al. 2016) proven that this method is robust enough for studying three-dimensional samples. Therefore, we decided to use it again in this study.

Comparing P–L relations for DCEPs and RR Lyr stars derived in this work with that found by Jacyszyn-Dobrzeniecka et al. (2016, 2017), we can see that  $a$  and  $b$  coefficients marginally differ. This is caused by using slightly different samples in these studies and this paper. Here we use the latest published version of the OGLE collection of pulsating stars (Soszyński et al., 2017), which was updated with a number of new objects as compared to the samples used by Jacyszyn-Dobrzeniecka et al. (2016, 2017). Additionally, the differences in P–L relations for DCEPs are caused by the fact that Jacyszyn-Dobrzeniecka et al. (2016) used multimode as well as single-mode pulsators to determine P–L relations, while in this study we only use single-mode stars.

The most up-to-date P–L relations for T2CEPs and ACEPs were published by Groenewegen & Jurkovic (2017b; see Table 1 on page 3). These relations are slightly different than ours (see Table 1). The reason for this discrepancy is that we use OGLE-IV collection of T2CEPs and ACEPs, while Groenewegen & Jurkovic (2017b) used data from the OGLE-III phase which covered significantly smaller area in the Magellanic System, i.e. did not include the LMC northern spiral arm. Therefore, this is the first time we present P–L relations based on the latest data.

In order to determine distances, we use the same method as Jacyszyn-Dobrzeniecka et al. (2016). However, we calculate distances separately for the LMC and SMC samples. Using appropriate P–L relation and period  $P$ , we calculate reference Wesenheit magnitude  $W_{\text{ref}}$  ( $a$  and  $b$  coefficients from Table 1):

$$W_{\text{ref}} = a \cdot \log(P) + b. \quad (3)$$

In the next step we calculate the relative distance modulus:

$$\delta\mu = W_I - W_{\text{ref}}, \quad (4)$$

and the absolute distance given as:

$$d = d_{\text{LMC/SMC}} \cdot 10^{\frac{\delta\mu}{5}}, \quad (5)$$

where  $d_{\text{LMC/SMC}}$  are the mean distances to the LMC ( $49.97 \pm 1.11$  kpc; Pietrzyński et al. 2013) and SMC ( $62.1 \pm 1.9$  kpc; Graczyk et al. 2014), respectively.

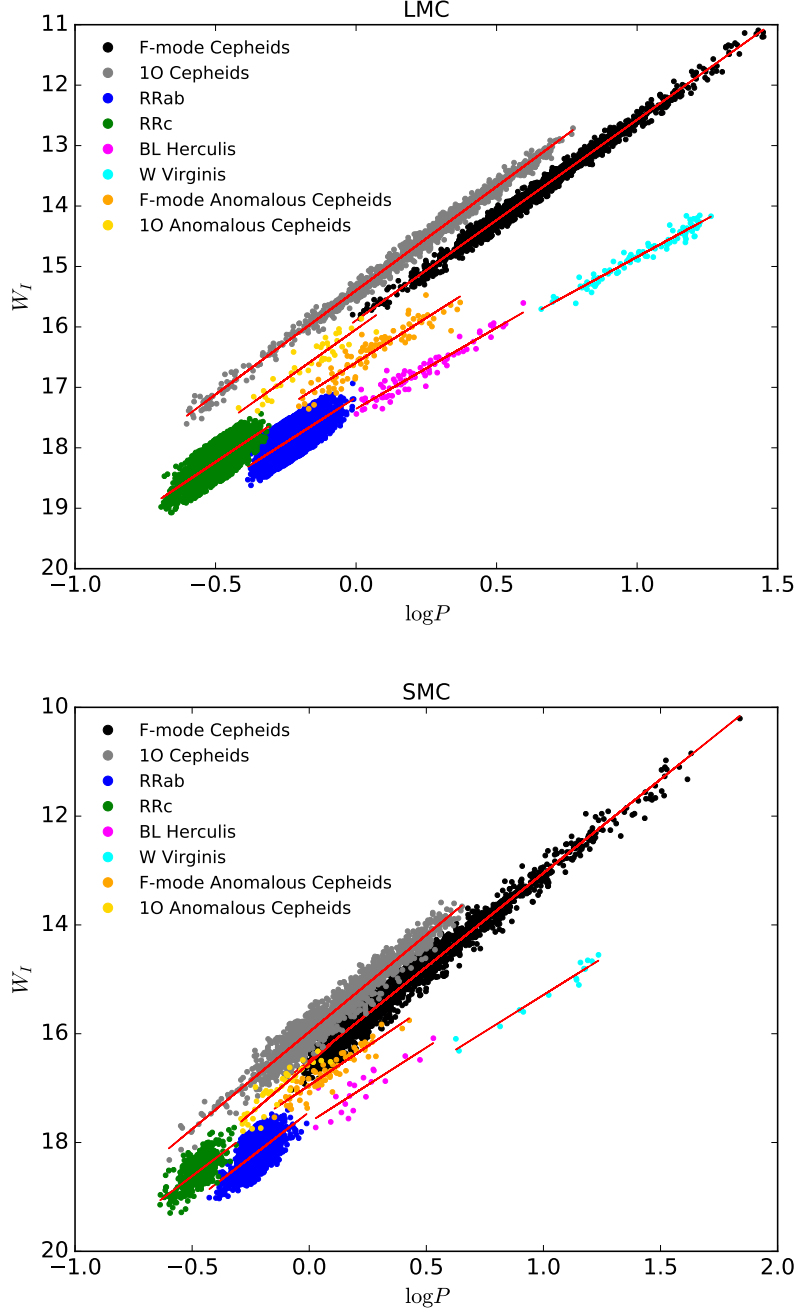


Figure 3: Period–luminosity diagrams for Classical Cepheids, Anomalous Cepheids, Type II Cepheids, and RR Lyrae variables in the Magellanic Clouds. We present P-L relations after all selection cuts and  $\sigma$ -clipping procedure.

## 4 Method of performing statistical tests

In order to compare three-dimensional distributions of pulsating stars from our collection we use the extended Kolmogorov-Smirnov (KS) statistical test. The two-sample two-dimensional version of the KS test was introduced by Peacock (1983), who found that this test is almost independent from the distribution type. This means that for large samples, critical values of the test statistics should not differ significantly. Gosset (1987) has extended the Peacock’s idea to three-dimensional distributions. The test statistic  $D_n$  is defined as the maximum absolute difference between two cumulative distribution functions. In three-dimensional space, 8 pairs of cumulative distribution functions are needed to calculate the test statistic  $D_n$ . Peacock (1983) pointed out that it was better to work with the test statistic  $Z_n$  defined as follow:

$$Z_n = \sqrt{\frac{n_1 n_2}{n_1 + n_2}} D_n, \quad (6)$$

where  $n_1$  and  $n_2$  are the sample sizes. Assuming that the first sample comes from the  $F(x, y, z)$  distribution, and the second sample comes from the  $G(x, y, z)$  distribution, we test the null ( $H_0$ ) and alternative ( $H_1$ ) hypotheses defined as follow:

$$\begin{aligned} H_0 : F(x, y, z) &= G(x, y, z), \\ H_1 : F(x, y, z) &\neq G(x, y, z), \end{aligned} \quad (7)$$

where  $H_0$  means that the analyzed samples come from the same distribution, while  $H_1$  means that samples come from different distributions.

The Peacock’s idea of the multidimensional, two-sample Kolmogorov-Smirnov test is implemented in the statistical software R (R Core Team, 2017). The package named “Peacock.test” (Xiao, 2016, 2017) allows calculating the test statistic  $D_n$  for two samples in two- and three-dimensional spaces. The test statistic  $D_n$  obtained in this calculation is converted to  $Z_n$  using the sample sizes  $n_1$  and  $n_2$ . Peacock (1983) determined that sizes of the tested samples  $n_1$  and  $n_2$  should be greater than 10, while Gosset (1987) indicated that the sample sizes must be greater than 5.

The main goal of this study is to examine similarities between spatial distributions of classical pulsators (DCEPs and RR Lyr variables) and T2CEPs or ACEPs. These similarities would allow us to better understand the nature of these stars, especially their possible evolutionary histories. We test all possible combinations of pairs of samples. Typically, the first sample with size  $n_1$  contains T2CEPs or ACEPs, while the second sample with size  $n_2$  consists of other classical pulsators. The groups of DCEPs or RR Lyr stars are much larger than other groups of pulsating stars. Therefore, we draw without returning a set of stars from classical pulsator distributions with size  $n_2$ , which is three times larger than  $n_1$ . We draw 1000 such samples, for which we compute the test statistics  $D_n$ , and later we convert it to  $Z_n$ . The statistical test for large samples requires a large amount of computational time, so we decided to count the tests repeatedly for smaller samples.

In their papers, Peacock (1983) and Gosset (1987) give empirical formulae for estimating probability  $p$  and testing the hypotheses. In the main part of our analysis, we use two-sided critical values of the “theoretical” test statistic  $Z_n$  for testing hypotheses and making decision whether to reject or accept  $H_0$ . However, we compare our decision-making method with asymptotic equations given by Gosset (1987). We discuss a comparison of these two methods in Section 6.

To test our hypotheses, we have to use the “theoretical” distribution of the test statistic in order to be able to compare this distribution (and its critical values) to the distribution of the test statistic of the tested samples. Bearing in mind the distribution-independent property of this test, we decide to use different “theoretical” distribution for each tested pair of samples. The sizes of the tested samples are not so large, therefore, the critical values of the test statistics are slightly different in each cases. Taking advantage of the fact that our collection of pulsating stars is very large, we decided to build a “theoretical” distributions of the test statistics based on all DCEPs and RR Lyr stars, with division into the pulsation mode. For example, to test the hypotheses for BL Her ( $n_1 = 79$ ) and RRab ( $n_2 = 3n_1 = 237$ ), we need “theoretical” distribution based only on RRab stars. Hence, we use RRab distribution to draw without returning samples with sizes  $n_1$  and  $n_2$ , which were tested 5000 times. We assume to test the hypotheses at the significance level of  $\alpha = 0.05$ . Therefore, for each „theoretical” distribution of  $Z_n$  we calculate 2.5th and 97.5th percentiles. The regions with  $Z_n$  smaller or equal than 2.5th percentile and larger or equal than 97.5th percentile are the *critical region* of the test statistic (region of the  $H_0$  rejection).

In the next step, we compare each  $Z_n$  calculated for our pulsating stars with critical values of the “theoretical” test statistic distribution. If the value of  $Z_n$  is in the critical region of the test statistic we conclude, that there are clear grounds to reject the null hypothesis  $H_0$ , so we have to accept alternative hypothesis  $H_1$ . However, when value  $Z_n$  is between 2.5th and 97.5th

percentiles we can conclude, that there is no sufficient evidence to reject the null hypothesis  $H_0$ , so we accept  $H_0$  (hence, we called this region *acceptability region*). We assumed that there is no evidence to reject  $H_0$  (and to indicate the possible similarity between two distributions) if at least 90% of the  $Z_n$  are in the region between critical values of the test statistics. Hence, we think that if over 900 test statistics are outside the rejection area, it is likely that we will be able to find similarity in the spatial distributions of stars.

To perform statistical tests, we transform equatorial coordinates and distances  $(\alpha, \delta, d)$  to the three-dimensional Cartesian space  $(x, y, z)$  with equations given by van der Marel & Cioni (2001) and Weinberg & Nikolaev (2001):

$$\begin{aligned} x &= -d \cdot \cos(\delta) \sin(\alpha - \alpha_{\text{cen}}), \\ y &= d \cdot (\sin(\delta) \cos(\delta_{\text{cen}}) - \cos(\delta) \sin(\delta_{\text{cen}}) \cos(\alpha - \alpha_{\text{cen}})), \\ z &= d \cdot (\cos(\delta) \cos(\delta_{\text{cen}}) \cos(\alpha - \alpha_{\text{cen}}) + \sin(\delta) \sin(\delta_{\text{cen}})). \end{aligned} \quad (8)$$

This transformation assumes that the observer is in  $(0, 0, 0)$  and the  $z$  axis is pointing toward the center of a Cloud at  $(\alpha_{\text{cen}}, \delta_{\text{cen}})$ . We transform LMC and SMC stars coordinates separately using the centers of the Magellanic Clouds based on the RR Lyr variables distributions (Jacyszyn-Dobrzniecka et al., 2017):

$$\begin{aligned} (\alpha_{\text{cen,LMC}}, \delta_{\text{cen,LMC}}) &= (5^{\text{h}}21^{\text{m}}31^{\text{s}}.2, -69^{\circ}36'36''), \\ (\alpha_{\text{cen,SMC}}, \delta_{\text{cen,SMC}}) &= (0^{\text{h}}55^{\text{m}}48^{\text{s}}.0, -72^{\circ}46'48''). \end{aligned} \quad (9)$$

To visualize and compare by eye stars distributions we use two-dimensional sky map in Hammer equal-area projection. We transform equatorial coordinates  $(\alpha, \delta)$  to coordinates in the Hammer system  $(x_{\text{Hammer}}, y_{\text{Hammer}})$ . In this coordinates transformation, the  $z$  axis is pointing toward  $(\alpha_{\text{cen}}, \delta_{\text{cen}}) = (3^{\text{h}}20^{\text{m}}, -72^{\circ})$ . Hammer coordinates are calculated as follow:

$$\begin{aligned} \alpha_{\text{b}} &= \alpha + \left(\frac{\pi}{2} - \alpha_{\text{cen}}\right), \\ l &= \arctan\left(\frac{\sin(\alpha_{\text{b}}) \cos(\delta_{\text{cen}}) + \tan(\delta) \sin(\delta_{\text{cen}})}{\cos(\alpha_{\text{b}})}\right) - \frac{1}{2}\pi, \\ \beta &= \arcsin(\sin(\delta) \cos(\delta_{\text{cen}}) - \cos(\delta) \sin(\delta_{\text{cen}}) \sin(\alpha_{\text{b}})), \\ x_{\text{Hammer}} &= -\frac{2\sqrt{2} \cos(\beta) \sin(\frac{l}{2})}{\sqrt{1 + \cos(\beta) \cos(\frac{l}{2})}}, \\ y_{\text{Hammer}} &= \frac{\sqrt{2} \sin(\beta)}{\sqrt{1 + \cos(\beta) \cos(\frac{l}{2})}}. \end{aligned} \quad (10)$$

Equations 8 and 10 are based on equations 7 – 14 from Jacyszyn-Dobrzniecka et al. (2016) though we applied a small correction to one of them. The version that we use here is presented above.

## 5 Results of our analysis

In Table 2 and 3, we present the results of statistical tests for all tested pairs of samples in the LMC, and SMC. Pairs of pulsating stars for which we can conclude similarity in their spatial distributions are marked in bold. All distributions of the test statistic  $Z_n$  in comparison to the “theoretical” distributions of the test statistic of the RR Lyr stars and DCEPs are presented in Figure 4 (for the LMC), and 5 (for the SMC). Using solid lines we marked from the left 2.5th, 50th (median), and 97.5th percentiles. The areas marked in gray are the rejection areas of the null hypothesis  $H_0$ .

In Figures 6-11, we present spatial distributions of T2CEPs and ACEPs in comparison to the DCEPs and RR Lyr variables distributions. We calculate test statistics for F-mode and 1O of ACEPs separately, but in the plots we present all these stars together, without dividing to the pulsation mode. We do this because the results for both pulsation modes are similar. We present only the most interesting cases for which results are similar in both Magellanic Clouds. In Figures 6-11, the top plot presents two-dimensional distributions of pulsating stars in the Magellanic Clouds in the equal-area Hammer projection (coordinates transformation described in Section 4). The middle and the bottom plots present  $xy$  (face-on view),  $xz$  (plan view) and  $yz$  (edge-on view) planes for the LMC, and the SMC, respectively. To estimate shapes of the galaxies in each projection we use standard kernel density estimation (KDE) based on the DCEPs or RR Lyr stars. The densest areas are marked in navy blue. Additionally, in each projection we plot normalized density contours.

The numbers of T2CEPs in the SMC are significantly smaller than in the LMC, therefore fitted P–L relations have larger uncertainties (see Table 1). Taking it into consideration tests may not be very accurate (despite the lower limit on the samples sizes, Peacock 1983; Gosset



1987, which is 10, and 5, respectively). Due to these reasons, we think that our analysis should be based mainly on the LMC, while SMC should be treated as an additional clue, not the foundation to drawing conclusions.

### 5.1 *BL Herculis*

Statistical tests in the LMC indicate, that the spatial distribution of BL Her and RR Lyr stars are similar (Fig. 4c, 4d, 6, 7). There are 92.5% and 93.0% of the test statistic in the acceptability region, for tests with RRab and RRc variables, respectively. This result is not surprising, because we expect that BL Her stars are old and have ages similar to the RR Lyr variables. Moreover, masses of the BL Her and RR Lyr stars are comparable (Groenewegen & Jurkovic, 2017a,b). In Figures 6 and 7, we can see that some BL Her stars in the LMC are concentrated in the center of the galaxy, but the vast majority of these objects are distributed out of the center creating a vast halo, which is typical for old populations. In the SMC, the statistical tests for BL Her stars with RR Lyr variables give comparable result. However, the difference is in the tests with DCEPs, for which we conclude similarities (Fig. 5a and 5b). As we mentioned before, it seems that this is due to small number of T2CEPs in the SMC. Moreover, it is difficult to compare by eye these two distributions in the SMC with such small number of BL Her variables. Our result coincides with the common knowledge about the evolution of BL Her stars.

### 5.2 *W Virginis*

Our statistical tests show that spatial distribution of W Vir stars is comparable with DCEPs in both Magellanic Clouds. The vast majority of the test statistics outside the rejection areas indicates that W Vir variables follow the distribution similar to that of young stars (Fig. 4e, 4f, 5e, 5f). The similarity of these two distributions is difficult to see in Figures 8 and 9, taking into account the fact that some of these stars are located in the area where there is a halo which consists of the old stars, and where young stars are practically absent. The most important question is whether the similarity of W Vir stars to DCEPs is related to the structures created by young population stars, i.e. the bar and spiral arms. The simplest test that can verify this thesis is to compare the spatial distribution of W Vir stars with RR Lyr variables, but with the limitation of the area in the three-dimensional space occupied by RR Lyr stars to the area occupied by DCEPs. We cut RR Lyr variables outskirts in the LMC to a sphere with the radius  $R = 5$  kpc, where the vast majority of DCEPs are located. In Figure 12 we present RR Lyr stars before and after the cut. Then we compared W Vir stars distribution with RRab variables distribution. In Figure 13, we present “theoretical” distribution in comparison to test statistic distribution for W Vir and RRab stars. After RRab halo cut, 94.0% of test statistics are outside the rejection area. This result suggests, that W Vir distribution similarities to DCEPs is not directly related to the structures created by the young population, but it is related to the lack of a big halo that RR Lyr stars have. Therefore, we are able to conclude that W Vir variables are intermediate-age stars with ages between DCEPs and RR Lyr variables, or they could be a mixture of old and intermediate-age stars.

### 5.3 *Anomalous Cepheids*

Distribution of ACEPs in the Magellanic Clouds differs from the distribution of DCEPs – all test statistics are in the rejection area of the null hypothesis (Fig. 4i, 4j, 4m, 4n, 5i, 5j, 5m, 5n). However, our tests indicate possible similarities in the distributions of these variables with RR Lyr stars (Fig. 4k, 4l, 4o, 4p, 5k, 5l, 5o, 5p). Unfortunately, we can not state the similarities in the spatial distributions of these stars for every considered case, because the percentage of test statistics outside the rejection area was below our  $H_0$  acceptability criterion. In the LMC, result for test of 10 ACEPs with RRc stars is close to our criterion, and it takes value 87.2%. The results are slightly different in the SMC, because in the case of 10 ACEPs we can state similarities to RRab and RRc distribution, but for F-mode ACEPs these similarities are only visible in comparison to RRab stars. In Figures 10 and 11, we present spatial distribution of ACEPs in comparison to the distributions of RRab, and RRc stars, respectively. It is clearly visible, that ACEPs form a vast halo-like old population in the LMC, and even larger halo than RR Lyr variables in the SMC. Hence, it seems that ACEPs belong to the old population.

## 6 Comparison of the decision making methods

Gosset (1987) provided asymptotic equations for estimating the probability  $p$  and making the decision about the hypotheses. These formulae are defined as follows:

$$1 - \frac{Z_n}{Z_\infty} = 0.75 \cdot \left( \frac{n_1 n_2}{n_1 + n_2} \right)^{-0.9}, \quad (11)$$

$$p \simeq 2 \exp(-3(Z_\infty - 1.05)^2).$$

By using them it is possible to calculate asymptotic value of test statistic  $Z_\infty$  for sample sizes  $n_1$  and  $n_2$  for which statistical test gives test statistic  $Z_n$ . We compare our results with the results obtained using Gossets' equations. As before, we assumed a significance level  $\alpha = 0.05$ . It means, that if  $p \leq 0.05$ , we have to reject the null hypothesis, but if  $p > 0.05$  there is no reason to reject the  $H_0$ , so we accept it. For testing hypotheses using Gossets' equations we decide to use significantly larger samples of classical pulsators. In general, we use all T2CEPs, ACEPs, and DCEPs. Due to the very long computational time needed for calculation test statistic for large samples in three-dimension space, we draw 2327 stars from RRab, and RRc LMC distributions. In the SMC, we use the same number of RRab variables, and entire sample of RRc stars.

In the LMC, we have almost 100% compliance of both decision-making methods. Only in the case of the 10 ACEPs and RRab stars the results are different. However, we find that Gossets' equations do not work well in every case (e.g., for tested pairs BL Her stars with RRab and RRc variables, probability  $p$  is greater than 1). In the SMC, we have differences in four pairs of testing samples.

It should be noted, that equations given by Gosset (1987) are only asymptotic approximations, therefore it is much better to rely on the critical values of the test statistic generated for the specific case. However, for simplified cases it is enough to use the equations given by Gosset (1987). Five different results out of all 32 tests give methods compatibility at 84%.

## 7 Conclusions

In this work, we compared three-dimensional distributions of various classical pulsators. We used the OGLE collection of DCEPs, T2CEPs, ACEPs and RR Lyr stars (Soszyński et al., 2015a,b, 2016, 2017, 2018), and period-luminosity relations which we separately fitted to each group of pulsating stars. To compare the spatial distributions, we used the extended Kolmogorov-Smirnov test (Peacock 1983; Gosset 1987; Xiao 2016, 2017). As a main decision-making method, we used specially prepared “theoretical” distributions, for which we counted critical values of the test statistics. We compared our method with the asymptotic formulae given by Gosset (1987). We omitted peculiar W Vir and RV Tau stars in the analysis, because the distances to them were determined with large uncertainty.

Our results show that BL Her stars have similar spatial distribution to that of RR Lyr variables. They clearly form a vast halo, like the old population. Moreover, four of BL Her stars from our sample are probable members of the LMC globular clusters (Soszyński et al., 2018). The masses of these variables are slightly smaller than those of RR Lyr stars. Additionally, every evolutionary scenario confirms evolution paths for BL Her. All results are consistent and allow us to conclude, that these stars have an age comparable to RR Lyr variables.

The comparison of the spatial distribution of W Vir stars to DCEPs and RR Lyr stars (also with halo cut, which is described in Section 5) suggests that the former variables are intermediate-age stars with age between DCEPs and RR Lyr stars. However, we found that one W Vir variable is a probable member of the LMC old globular cluster (Soszyński et al., 2018). For this reason, we are more inclined to conclude that these variables are a mixture of old and intermediate-age stars. An additional argument for this can be the masses of W Vir stars – they are comparable to BL Her stars masses (Groenewegen & Jurkovic, 2017b). Moreover, following this we can also state that they are comparable to RR Lyr stars masses. Unfortunately, there is still no convincing evolutionary model that can explain the origin and evolution of W Vir stars, especially blue loops through the instability strip.

Previous studies of the spatial distribution of ACEPs show that it is different than distributions of DCEPs or RR Lyr (Fiorentino & Monelli, 2012). For ACEPs in the Magellanic Clouds we can conclude with great certainty that three-dimensional distribution of these stars is completely different than distribution of DCEPs. The statistical tests of the spatial distribution of these stars with RR Lyr variables do not give clear conclusions, because not all results meet our  $H_0$  acceptability criterion. However, the percentage of the test statistics outside the critical regions allows us to conclude, that ACEPs are stars belonging to the old population. This conclusion is confirmed by the vast halo that these stars form in the Magellanic Clouds. Ages similar to the RR Lyr variables suggest that the most favorable evolution scenario for these stars is coalescence of two low-mass stars in the binary system. If these stars evolved as a single one, they should be definitely younger.

The similarities of the three-dimensional distributions of T2CEPs and ACEPs to the other classical pulsators distributions give us clues about the origin of these stars and their properties. However, we cannot forget that it is only a statistical method, which is burdened with numerous assumptions. In the SMC, differences in the distributions of the pulsating stars, compared with the LMC, are visible by the naked eye. Therefore, we do not expect that the compliance for both Magellanic Clouds will be at 100%. Due to the greater number of such stars in the LMC, we suggest to base the analysis on this galaxy.

## 8 Acknowledgements

The authors would like to thank M. Marconi and M. Groenewegen for a fruitful discussion and valuable comments during 4th MIAPP programme 2018 “The Extragalactic Distance Scale in the Gaia Era” which took place from 11th June to 6th July 2018, in Garching, Germany. The authors are also grateful to J. A. Peacock and Y. Xiao for advice regarding the idea of an multidimensional Kolmogorov-Smirnov test and its implementation in the R software.

This work has been supported by the National Science Centre, Poland, grant MAESTRO no. 2016/22/A/ST9/00009 to I. Soszyński. P. Iwanek is partially supported by the “Kartezjusz” programme no. POWR.03.02.00-00-I001/16-00 founded by The National Centre for Research and Development, Poland. The OGLE project has received funding from the National Science Center, Poland, grant MAESTRO no. 2014/14/A/ST9/00121 to A. Udalski.

Table 2: Results of the statistical tests in the Large Magellanic Cloud. Pairs of pulsating stars for which we can conclude similarity in their spatial distributions are marked in bold.

| tested samples ( $n_1$ and $n_2$ )                      | LMC          |       |                               |       |        |                                       |                           | decision                         |
|---|--------------|-------|-------------------------------|-------|--------|---------------------------------------|---------------------------|----------------------------------|
|   | sample sizes |       | „theoretical” test statistics |       |        | test statistics of the tested samples |                           |                                  |
|   | $n_1$        | $n_2$ | 2.5th                         | 50th  | 97.5th | % $Z_n$ in crit. region               | % $Z_n$ in accept. region |                                  |
| BL Hercules and F-mode Cepheids (Fig. 4a)               | 79           | 237   | 1.234                         | 1.624 | 2.176  | 100.00                                | 0.00                      | $H_0$ rejected                   |
| BL Hercules and 1O Cepheids (Fig. 4b)                   |              |       | 1.202                         | 1.591 | 2.144  | 98.80                                 | 1.20                      | $H_0$ rejected                   |
| <b>BL Hercules and RRab (Fig. 4c)</b>                   |              |       | 1.267                         | 1.656 | 2.209  | <b>7.50</b>                           | <b>92.50</b>              | <b><math>H_0</math> accepted</b> |
| <b>BL Hercules and RRc (Fig. 4d)</b>                    |              |       | 1.267                         | 1.656 | 2.209  | <b>7.00</b>                           | <b>93.00</b>              | <b><math>H_0</math> accepted</b> |
| <b>W Virginis and F-mode Cepheids (Fig. 4e)</b>         | 94           | 282   | 1.251                         | 1.608 | 2.144  | <b>6.10</b>                           | <b>93.90</b>              | <b><math>H_0</math> accepted</b> |
| <b>W Virginis and 1O Cepheids (Fig. 4f)</b>             |              |       | 1.221                         | 1.578 | 2.114  | <b>9.30</b>                           | <b>90.70</b>              | <b><math>H_0</math> accepted</b> |
| W Virginis and RRab (Fig. 4g)                           |              |       | 1.280                         | 1.667 | 2.233  | 80.10                                 | 19.90                     | $H_0$ rejected                   |
| W Virginis and RRc (Fig. 4h)                            |              |       | 1.251                         | 1.667 | 2.203  | 77.60                                 | 22.40                     | $H_0$ rejected                   |
| F-mode Anomalous Cepheids and F-mode Cepheids (Fig. 4i) | 94           | 282   | 1.251                         | 1.608 | 2.144  | 100.00                                | 0.00                      | $H_0$ rejected                   |
| F-mode Anomalous Cepheids and 1O Cepheids (Fig. 4j)     |              |       | 1.221                         | 1.578 | 2.114  | 100.00                                | 0.00                      | $H_0$ rejected                   |
| F-mode Anomalous Cepheids and RRab (Fig. 4k)            |              |       | 1.280                         | 1.667 | 2.233  | 41.20                                 | 58.80                     | $H_0$ rejected                   |
| F-mode Anomalous Cepheids and RRc (Fig. 4l)             |              |       | 1.251                         | 1.667 | 2.203  | 42.20                                 | 57.80                     | $H_0$ rejected                   |
| 1O Anomalous Cepheids and F-mode Cepheids (Fig. 4m)     | 39           | 117   | 1.202                         | 1.618 | 2.126  | 100.00                                | 0.00                      | $H_0$ rejected                   |
| 1O Anomalous Cepheids and 1O Cepheids (Fig. 4n)         |              |       | 1.202                         | 1.572 | 2.173  | 100.00                                | 0.00                      | $H_0$ rejected                   |
| 1O Anomalous Cepheids and RRab (Fig. 4o)                |              |       | 1.248                         | 1.618 | 2.173  | 17.00                                 | 83.00                     | $H_0$ rejected                   |
| 1O Anomalous Cepheids and RRc (Fig. 4p)                 |              |       | 1.248                         | 1.618 | 2.173  | 12.80                                 | 87.20                     | $H_0$ rejected                   |

Table 3: Results of the statistical tests in the Small Magellanic Cloud. Pairs of pulsating stars for which we can conclude similarity in their spatial distributions are marked in bold.

| tested samples ( $n_1$ and $n_2$ )                      | SMC          |       |                               |       |        |                                       |                           | decision                         |
|---|--------------|-------|-------------------------------|-------|--------|---------------------------------------|---------------------------|----------------------------------|
|   | sample sizes |       | „theoretical” test statistics |       |        | test statistics of the tested samples |                           |                                  |
|   | $n_1$        | $n_2$ | 2.5th                         | 50th  | 97.5th | % $Z_n$ in crit. region               | % $Z_n$ in accept. region |                                  |
| <b>BL Herculis and F-mode Cepheids (Fig. 5a)</b>        | 20           | 60    | 1.162                         | 1.549 | 2.130  | <b>0.60</b>                           | <b>99.40</b>              | <b><math>H_0</math> accepted</b> |
| <b>BL Herculis and 1O Cepheids (Fig. 5b)</b>            |              |       | 1.162                         | 1.549 | 2.066  | <b>0.90</b>                           | <b>99.10</b>              | <b><math>H_0</math> accepted</b> |
| <b>BL Herculis and RRab (Fig. 5c)</b>                   |              |       | 1.225                         | 1.549 | 2.130  | <b>1.60</b>                           | <b>98.40</b>              | <b><math>H_0</math> accepted</b> |
| <b>BL Herculis and RRc (Fig. 5d)</b>                    |              |       | 1.162                         | 1.549 | 2.066  | <b>1.00</b>                           | <b>99.00</b>              | <b><math>H_0</math> accepted</b> |
| <b>W Virginis and F-mode Cepheids (Fig. 5e)</b>         | 15           | 45    | 1.193                         | 1.491 | 2.012  | <b>9.60</b>                           | <b>90.40</b>              | <b><math>H_0</math> accepted</b> |
| <b>W Virginis and 1O Cepheids (Fig. 5f)</b>             |              |       | 1.193                         | 1.565 | 2.012  | <b>8.60</b>                           | <b>91.40</b>              | <b><math>H_0</math> accepted</b> |
| W Virginis and RRab (Fig. 5g)                           |              |       | 1.193                         | 1.565 | 2.087  | 14.90                                 | 85.10                     | $H_0$ rejected                   |
| W Virginis and RRc (Fig. 5h)                            |              |       | 1.193                         | 1.565 | 2.012  | 25.60                                 | 74.40                     | $H_0$ rejected                   |
| F-mode Anomalous Cepheids and F-mode Cepheids (Fig. 5i) | 72           | 216   | 1.225                         | 1.599 | 2.177  | 100.00                                | 0.00                      | $H_0$ rejected                   |
| F-mode Anomalous Cepheids and 1O Cepheids (Fig. 5j)     |              |       | 1.191                         | 1.599 | 2.143  | 100.00                                | 0.00                      | $H_0$ rejected                   |
| <b>F-mode Anomalous Cepheids and RRab (Fig. 5k)</b>     |              |       | 1.259                         | 1.633 | 2.211  | <b>8.90</b>                           | <b>91.10</b>              | <b><math>H_0</math> accepted</b> |
| F-mode Anomalous Cepheids and RRc (Fig. 5l)             |              |       | 1.157                         | 1.497 | 2.007  | 34.80                                 | 65.20                     | $H_0$ rejected                   |
| 1O Anomalous Cepheids and F-mode Cepheids (Fig. 5m)     | 39           | 117   | 1.202                         | 1.572 | 2.126  | 100.00                                | 0.00                      | $H_0$ rejected                   |
| 1O Anomalous Cepheids and 1O Cepheids (Fig. 5n)         |              |       | 1.202                         | 1.572 | 2.126  | 100.00                                | 0.00                      | $H_0$ rejected                   |
| <b>1O Anomalous Cepheids and RRab (Fig. 5o)</b>         |              |       | 1.248                         | 1.618 | 2.173  | <b>1.30</b>                           | <b>98.70</b>              | <b><math>H_0</math> accepted</b> |
| <b>1O Anomalous Cepheids and RRc (Fig. 5p)</b>          |              |       | 1.202                         | 1.525 | 2.034  | <b>1.10</b>                           | <b>98.90</b>              | <b><math>H_0</math> accepted</b> |

## LMC

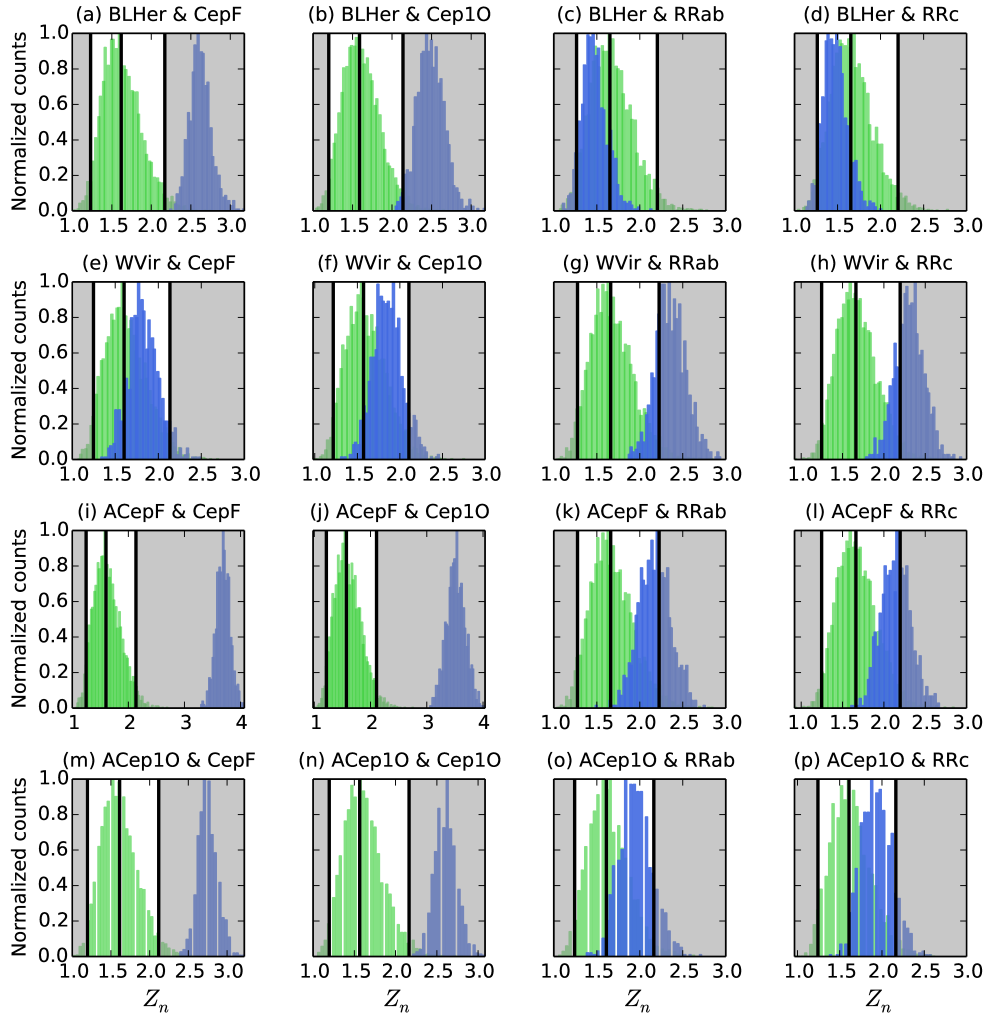


Figure 4: Distributions of the test statistic  $Z_n$  for each tested pair of samples from the Large Magellanic Cloud. With green color we marked “theoretical” distributions of the test statistic built based on Classical Cepheids and RR Lyraes, while blue histograms show the test statistic obtained during the test spatial distributions of Type II Cepheids and Anomalous Cepheids with other classical pulsators. With solid, black lines we marked percentiles 2.5th, 50th (median), and 97.5th (from left side respectively). The area marked in gray is the null hypothesis rejection area (critical region of the test statistic). Each plot represents different pair of tested samples.

## SMC

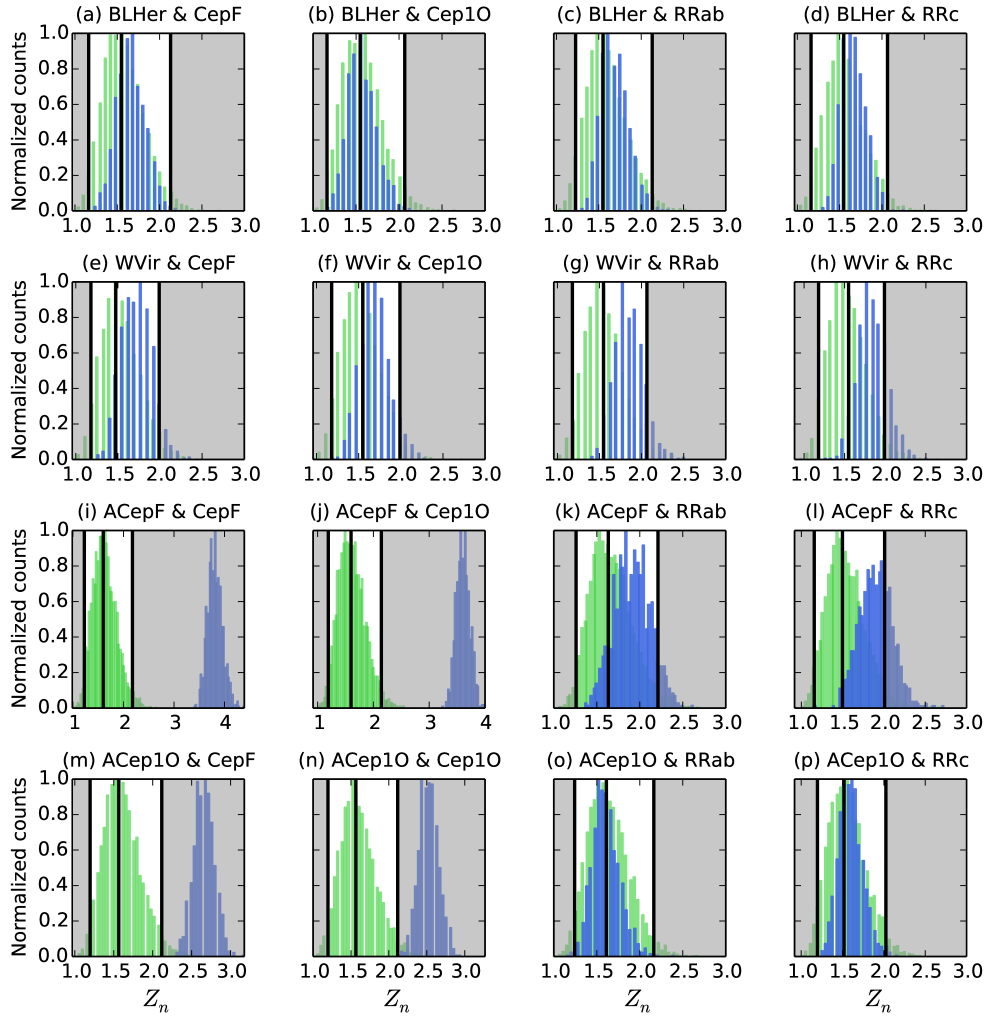


Figure 5: Distributions of the test statistic  $Z_n$  for each tested pair of samples from the Small Magellanic Cloud. With green color we marked „theoretical” distributions of the test statistic built based on classical Cepheids and RR Lyraes, while blue histograms show the test statistic obtained during the test spatial distributions of Type II Cepheids and Anomalous Cepheids with other classical pulsators. With solid, black lines we marked percentiles 2.5th, 50th (median), and 97.5th (from left side respectively). The area marked in gray is the null hypothesis rejection area (critical region of the test statistic). Each plot represents different pair of tested samples.

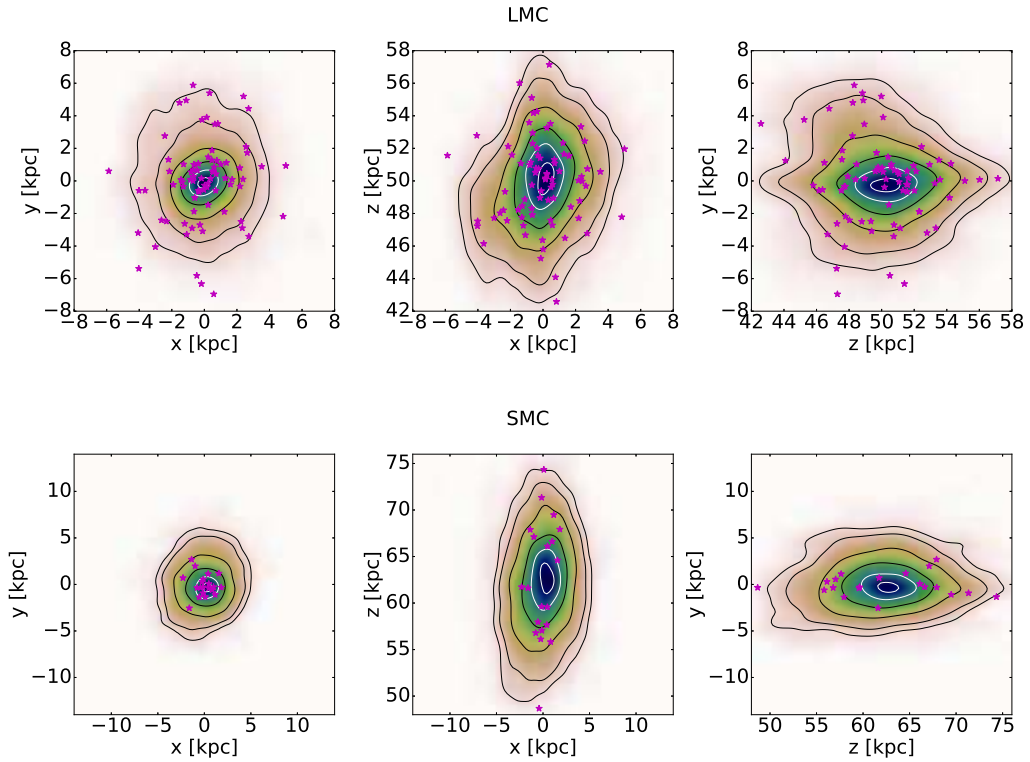
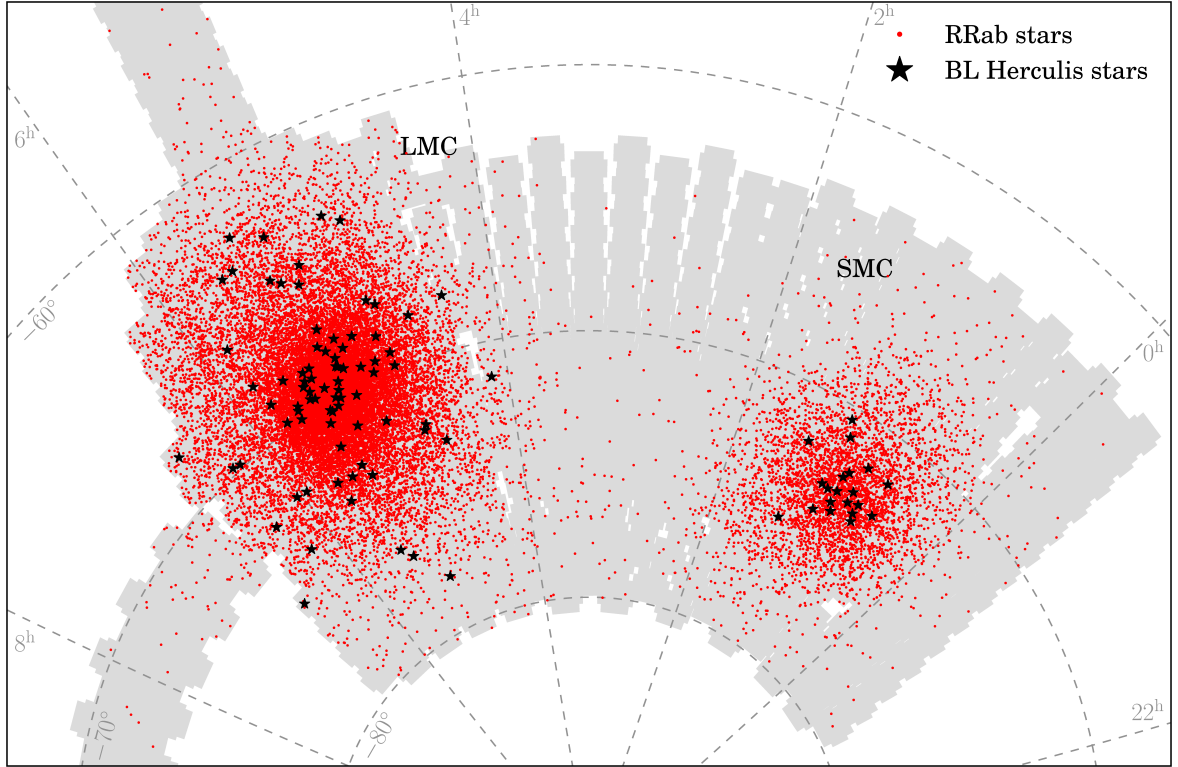


Figure 6: Spatial distribution of BL Her stars in comparison to the distribution of RRab stars. Top panel presents equal-area Hammer projection of the Magellanic System. Area marked in gray is the OGLE-IV footprint. Middle and bottom panels present Cartesian projections for the LMC and the SMC, respectively. We estimate shapes of the galaxies in each projection using standard kernel density estimation (KDE) and RRab stars, which are marked with color map. Additionally, in each projection we plot normalized density contours. From the center of the galaxies to the edge, we plot normalized density with value: 95% (first white contour), 75% (second white contour), 50%, 25%, 10% and 5%. With magenta points, we marked BL Her stars.



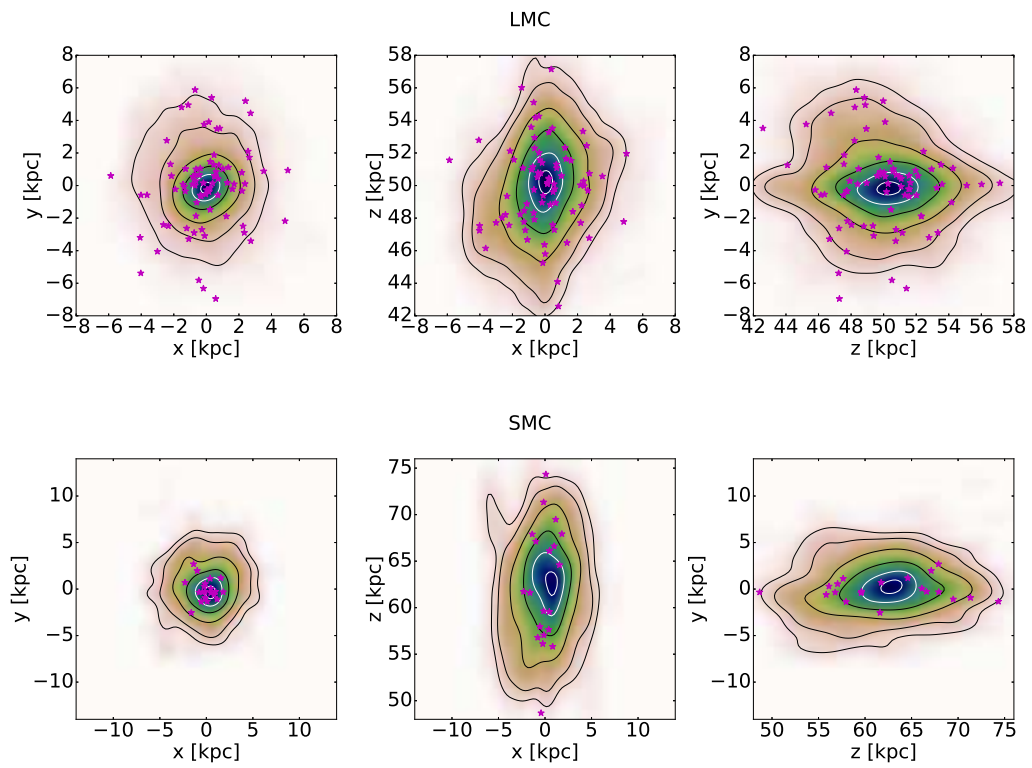
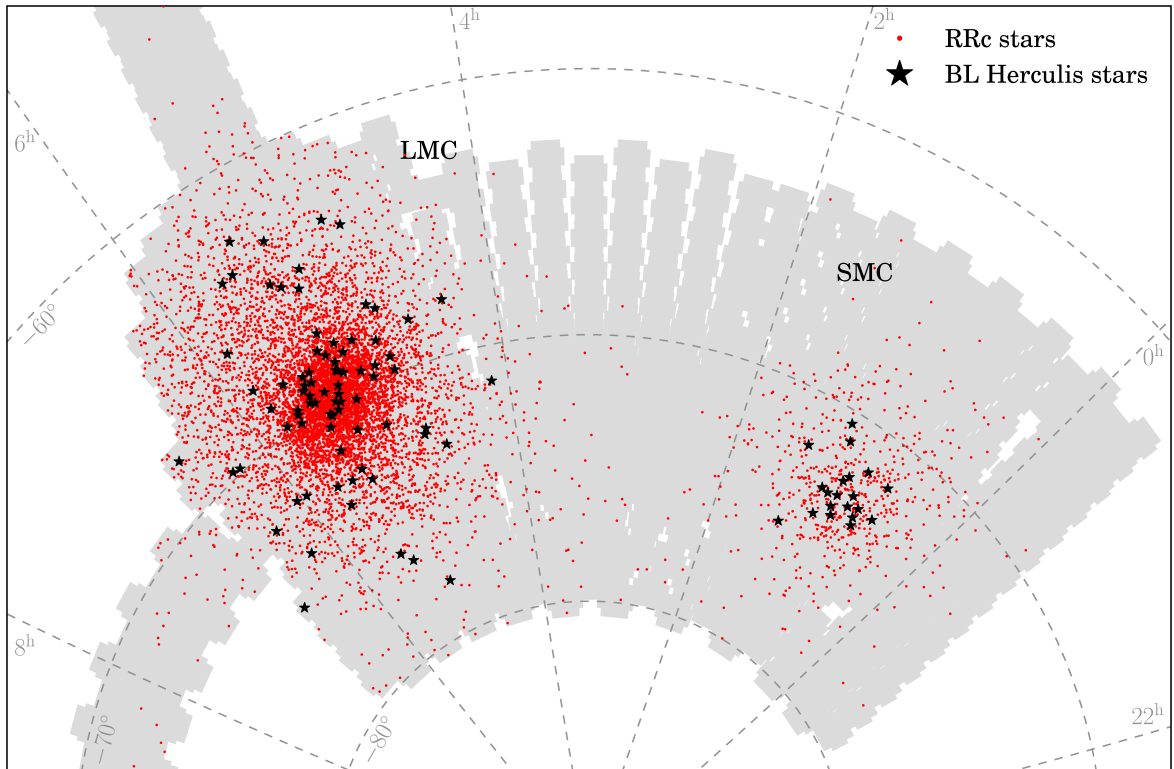


Figure 7: Same as Fig. 6, but for BL Her and RRc stars.

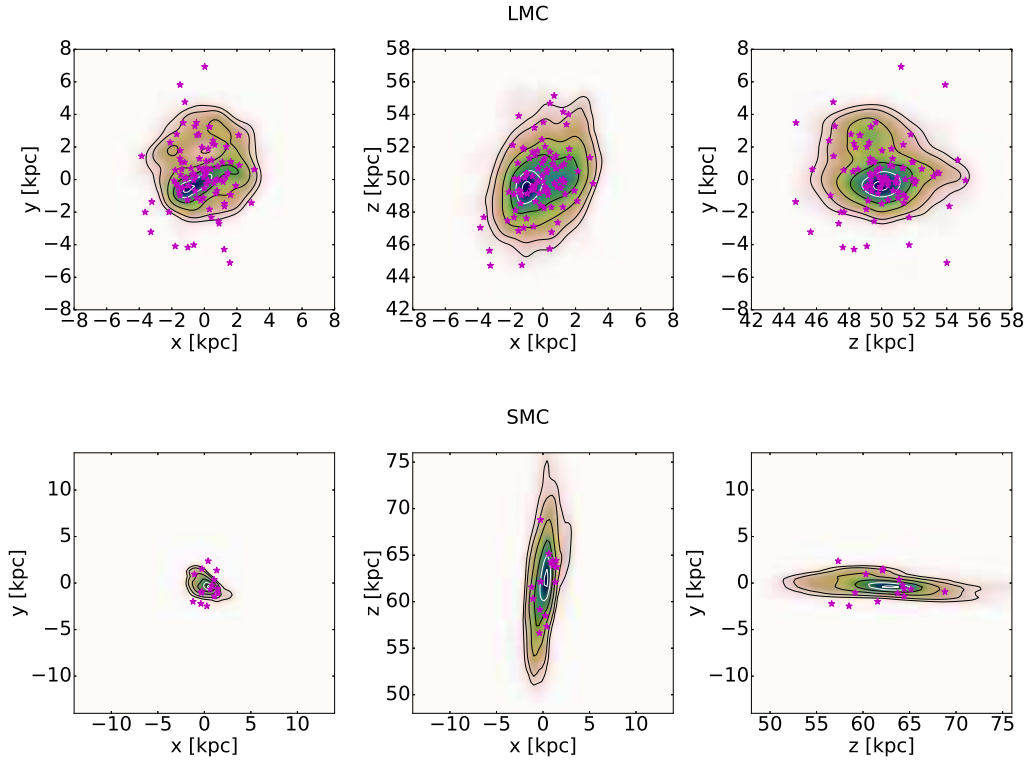
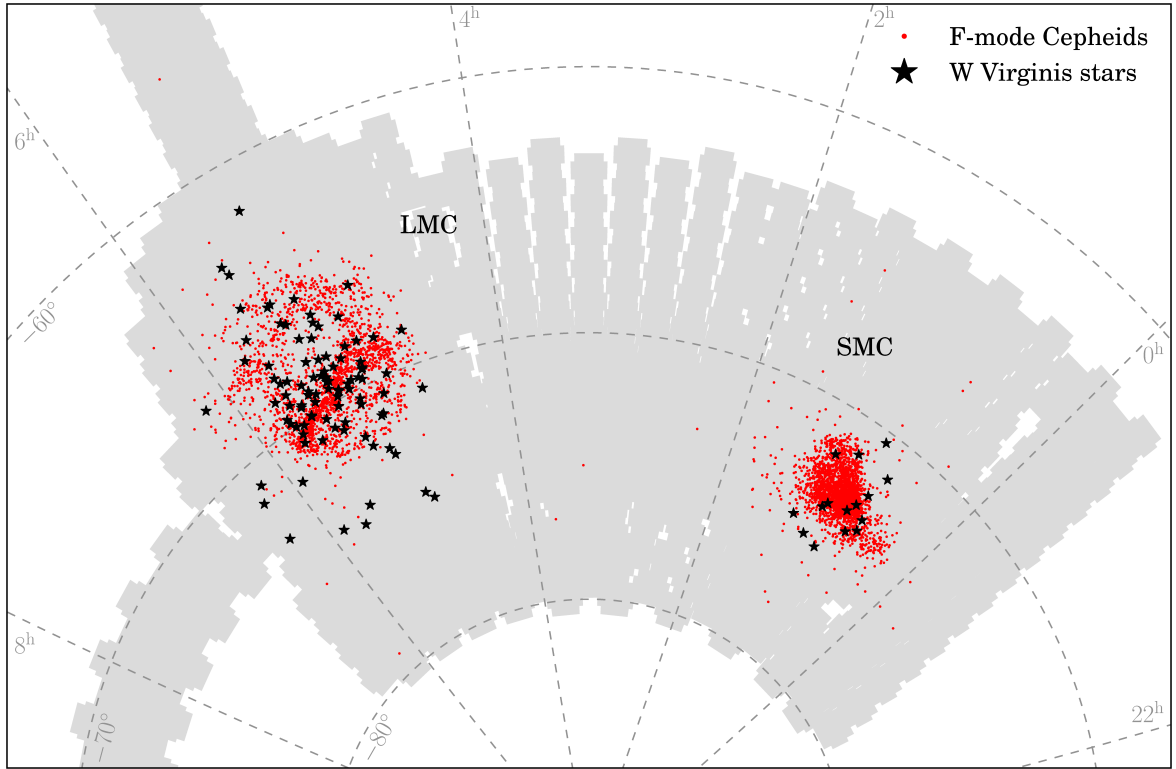


Figure 8: Same as Fig. 6, but for W Vir stars and F-mode Cepheids.

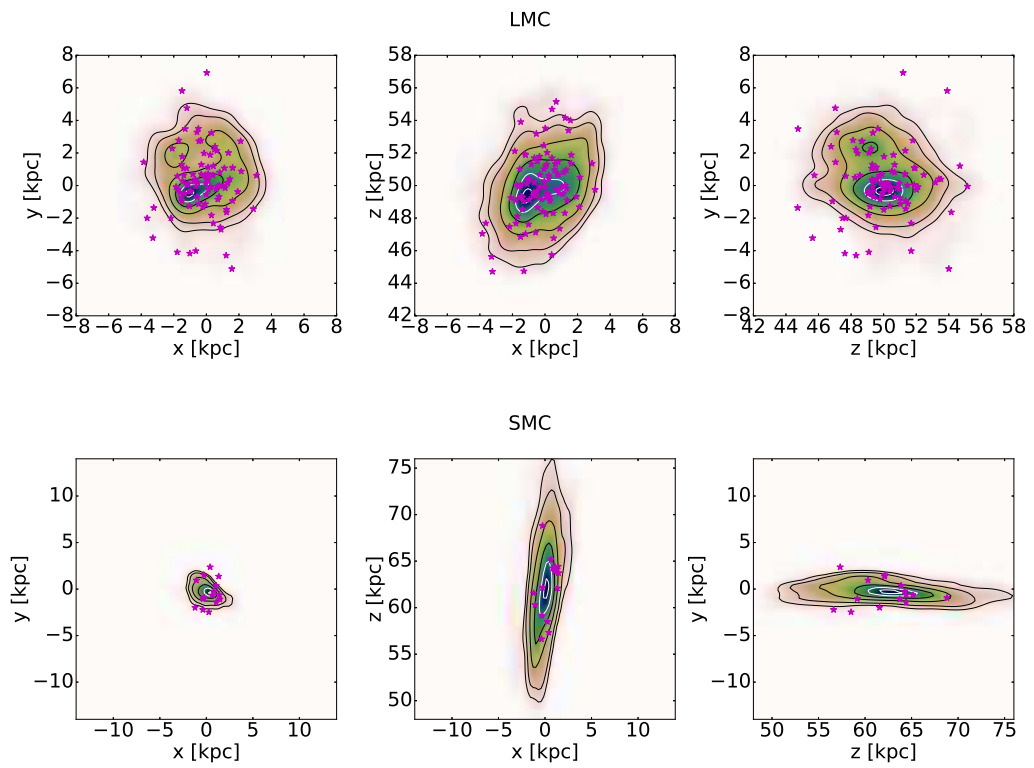
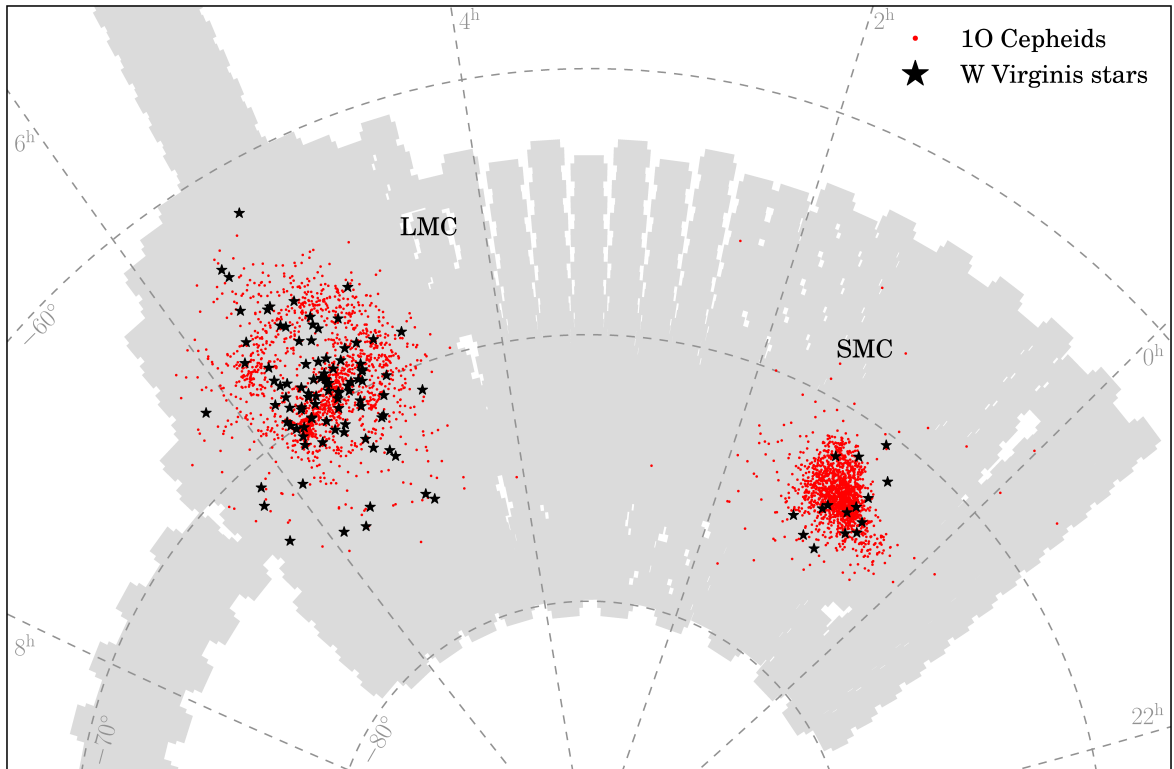


Figure 9: Same as Fig. 6, but for W Vir stars and 10 Cepheids.

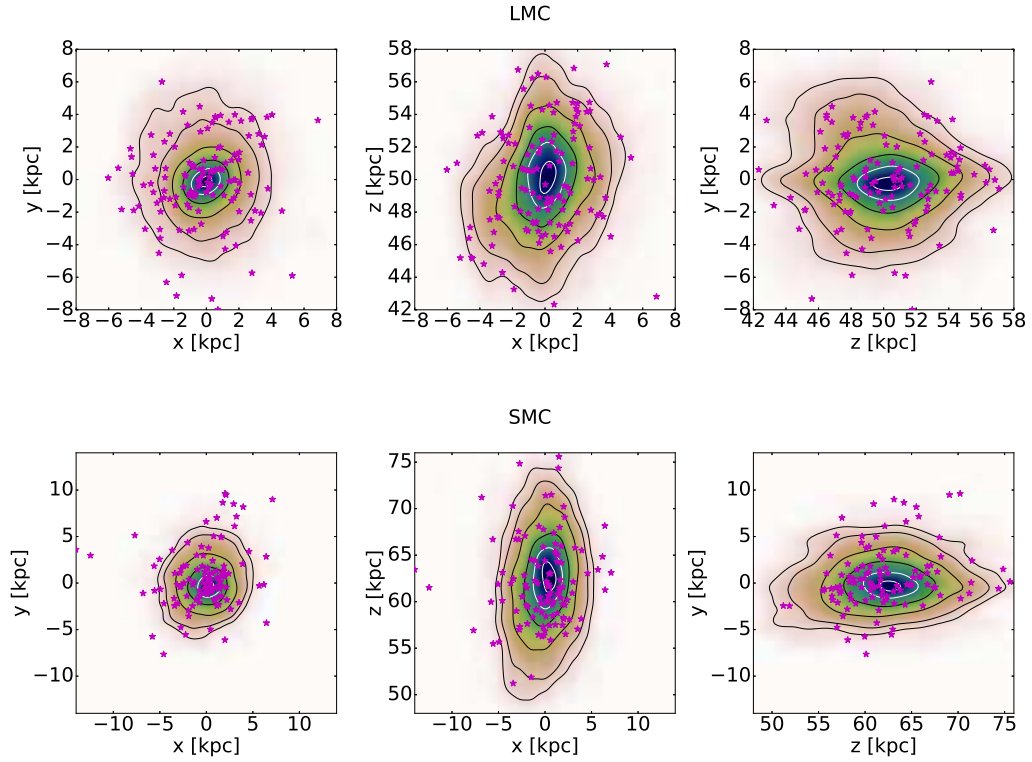
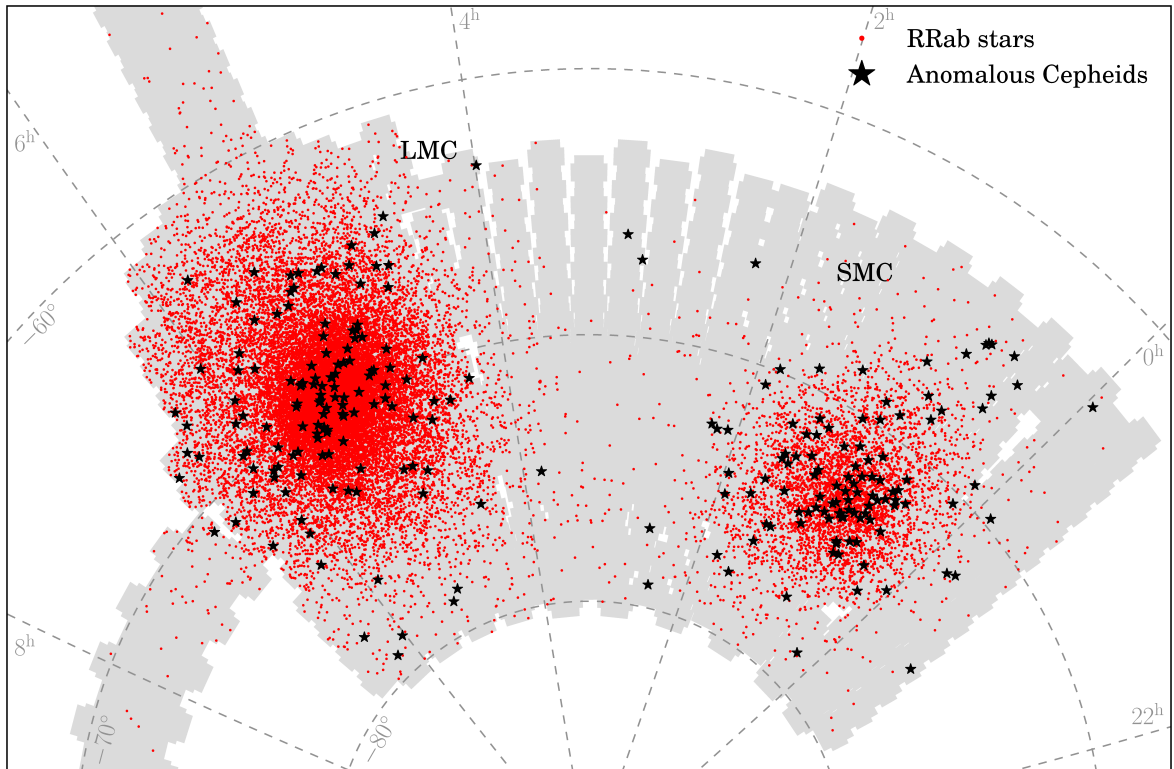


Figure 10: Same as Fig. 6, but for Anomalous Cepheids and RRab stars.

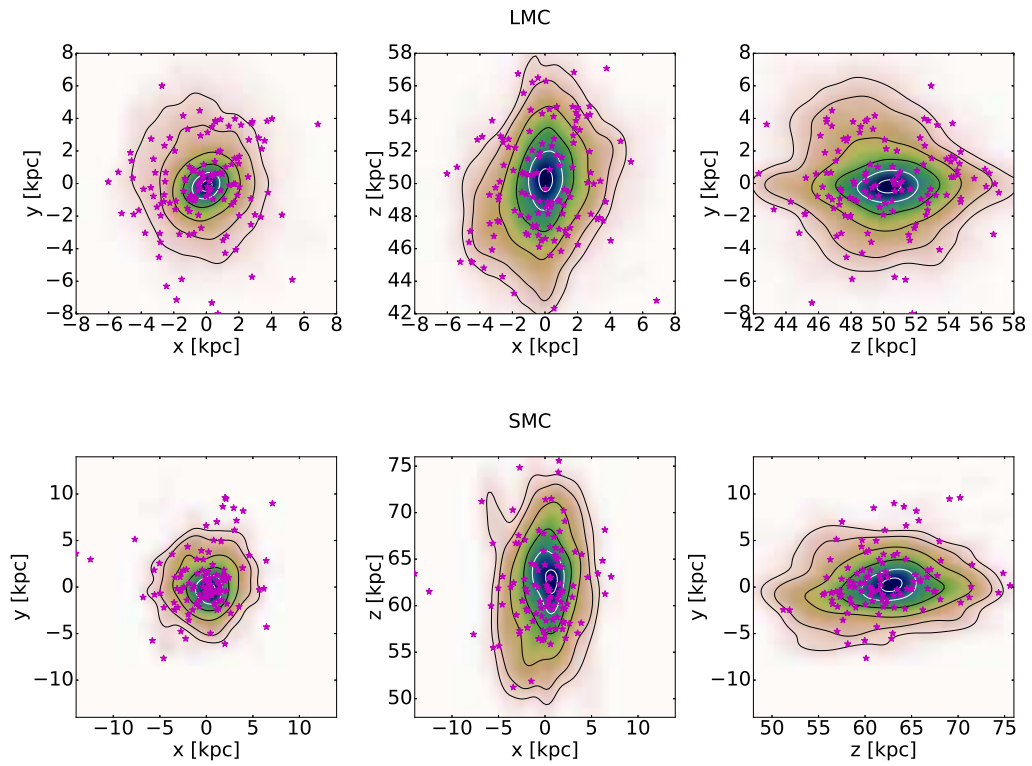
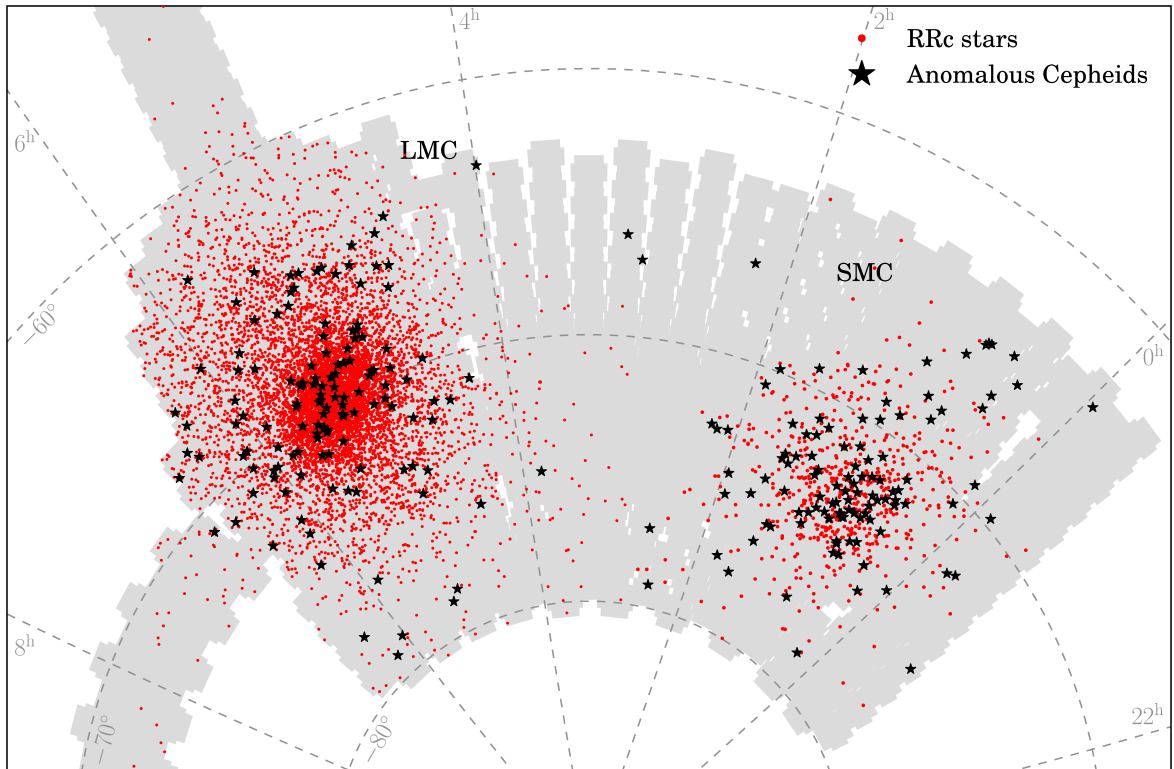


Figure 11: Same as Fig. 6, but for Anomalous Cepheids and RRc stars.

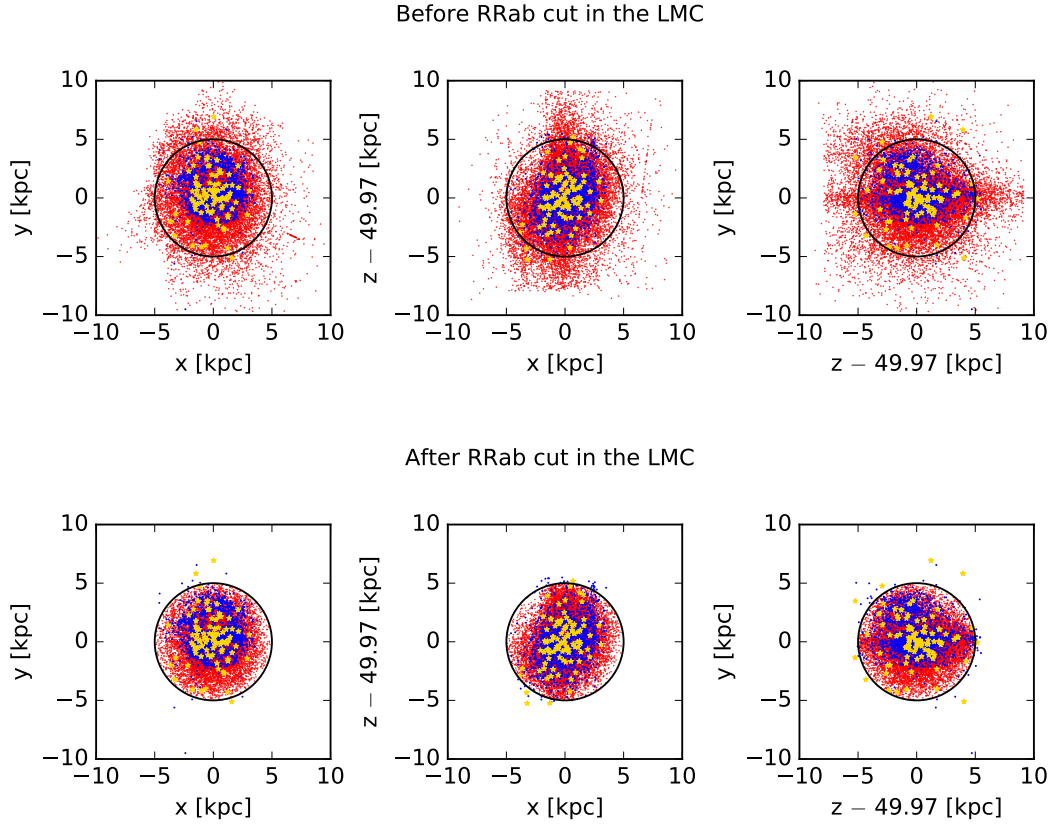


Figure 12: Cutting procedure for RRab outskirts regions in the Large Magellanic Cloud. With red dots we marked RRab stars, blue dots correspond to F-mode Cepheids, while gold stars present W Vir distribution. Black circles represent the cut boundary of the RRab stars halo, at the radius  $R = 5$  kpc.

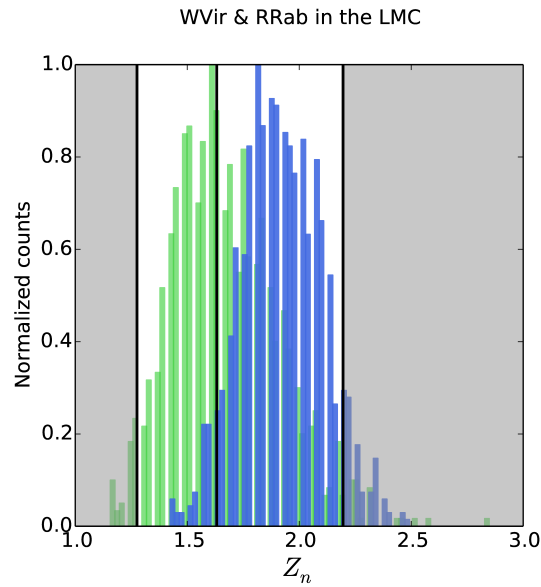


Figure 13: Distribution of the test statistic  $Z_n$  for statistical test of W Vir stars with RRab variables after the cut of outskirts regions in the Large Magellanic Cloud.

## References

- Baade W., 1952, *Trans. I.A.U.*, 8, 397
- Cassisi S., Salaris M., 2013, *Old Stellar Populations: How to Study the Fossil Record of Galaxy Formation*
- Deb S., Ngeow C.-C., Kanbur S. M., Singh H. P., Wysocki D., Kumar S., 2018, *MNRAS*, 478, 2526
- Fiorentino G., Monelli M., 2012, *A&A*, 540, A102
- Gingold R. A., 1976, *ApJ*, 204, 116
- Gingold R. A., 1985, *MmSAI*, 56, 169
- Gosset E., 1987, *A&A*, 188, 258
- Graczyk D., et al., 2014, *ApJ*, 780, 59
- Groenewegen M. A. T., Jurkovic M. I., 2017a, *A&A*, 603, A70
- Groenewegen M. A. T., Jurkovic M. I., 2017b, *A&A*, 604, A29
- Inno L., et al., 2016, *ApJ*, 832, 176
- Jacyszyn-Dobrzeniecka A. M., et al., 2016, *Acta Astron.*, 66, 149
- Jacyszyn-Dobrzeniecka A. M., et al., 2017, *Acta Astron.*, 67, 1
- Leavitt H. S., Pickering E. C., 1912, *HarCi*, 173, 1
- Madore B. F., 1976, in *The Galaxy and the Local Group*. p. 153
- Matsunaga N., Feast M. W., Menzies J. W., 2009, *MNRAS*, 397, 933
- Nikolaev S., Drake A. J., Keller S. C., Cook K. H., Dalal N., Griest K., Welch D. L., Kanbur S. M., 2004, *ApJ*, 601, 260
- Peacock J. A., 1983, *MNRAS*, 202, 615
- Pietrzyński G., et al., 2013, *Natur*, 495, 76
- R Core Team 2017, *R: A Language and Environment for Statistical Computing*. R Foundation for Statistical Computing, Vienna, Austria, <https://www.R-project.org/>
- Schlegel D. J., Finkbeiner D. P., Davis M., 1998, *ApJ*, 500, 525
- Soszyński I., et al., 2008, *Acta Astron.*, 58, 293
- Soszyński I., et al., 2015a, *Acta Astron.*, 65, 233
- Soszyński I., et al., 2015b, *Acta Astron.*, 65, 297
- Soszyński I., et al., 2016, *Acta Astron.*, 66, 131
- Soszyński I., et al., 2017, *Acta Astron.*, 67, 103
- Soszyński I., et al., 2018, *Acta Astron.*, 68, 89
- Thackeray A. D., 1950, *Obs*, 70, 144
- Udalski A., Szymański M. K., Szymański G., 2015, *Acta Astron.*, 65, 1
- Weinberg M. D., Nikolaev S., 2001, *ApJ*, 548, 712
- Welch D. L., 2012, *JAVSO*, 40, 492
- Xiao Y., 2016, *Peacock.test: Two and Three Dimensional Kolmogorov-Smirnov Two-Sample Tests*. <https://CRAN.R-project.org/package=Peacock.test>
- Xiao Y., 2017, *Comput. Stat. Data Anal.*, 105, 53
- Zinn R., Searle L., 1976, *ApJ*, 209, 734
- van der Marel R. P., Cioni M.-R. L., 2001, *AJ*, 122, 1807